

Persistence Curves: A Canonical Framework for Summarizing Persistence Diagrams

Yu-Min Chung (y.chung@uncg.edu) and
Austin Lawson (azlawson@uncg.edu)
UNC Greensboro

Abstract

Persistence diagrams are one of the main tools in the field of Topological Data Analysis (TDA). They contain fruitful information about the shape of data. The use of machine learning algorithms on the space of persistence diagrams proves to be challenging as the space is complicated. For that reason, transforming these diagrams in a way that is compatible with machine learning is an important topic currently researched in TDA. In this paper, our main contribution consists of three components. First, we develop a general framework of vectorizing diagrams that we call the *Persistence Curves* (PCs). We show that some well-known summaries, such as Betti number curves, the Euler Characteristic Curve, and Persistence Landscapes fall under the PC framework or are easily derived from it. Second, we provide a theoretical foundation for the stability analysis of PCs. In addition, we propose several new summaries based on PC framework and investigate their stability. Finally, we demonstrate the practical uses of PCs on the texture classification on four public available texture datasets. We show the result of our proposed PCs outperforms several existing TDA methods.

1 Introduction

Topological data analysis (TDA) is a relatively new field of mathematics that seeks to examine the shape and structure of data. Persistent homology (PH) is an important tool in TDA developed in the early 2000s [23, 52, 56] based on the work of size functions [25, 26]. Since its inception, TDA has permeated through many disciplines such as neuroscience [5], medical biology [36], sensor networks [20], social networks [12], physics [21], computation [39], nanotechnology [41], and material science [53].

Generally speaking, persistent homology concerns the shape of a sequence of topological spaces with a nested subset relation, called a filtration. It tracks when topological features appear (are born) and disappear (die). Collecting this birth-death information leads to a visual summary called a *persistence diagram*. The amount of time a topological feature exists, called its lifespan. Intuitively,

the lifespan indicates the relative importance of the associated feature. As is the case for all rules of thumb, this one has exceptions. For example, in [5], it was found that the 28th longest lifespan was the most informative. Analyzing persistence diagrams is a fundamental task in TDA. It has been shown by [40] that the space of persistence diagrams is a complete and separable metric space with the so-called Wasserstein distance. However, the space presents a great challenge for one to apply machine learning methods directly. For instance, as shown in [40], the mean of the persistence diagrams may not be unique. This motivates researchers to transform persistence diagrams into some spaces more palatable for these analytic methods. There are some common approaches to summarize persistence diagrams, including kernel functions and vectorization. In the former, one constructs a kernel function, or a rule for measuring and quantifying the likeness of two persistence diagrams. This approach has been seen through a bag-of-words approach [35], kernel SVM for persistence [49], persistence intensity functions [15], and persistence weighted Gaussian kernel [32]. On the other hand, to vectorize a persistence diagram is to map it into a vector space, usually \mathbb{R}^n . The vectorization of persistence diagrams has proven quite popular in recent literature and we can find this summarization type in the form of persistence landscapes [8], persistence images [1], persistence indicator functions [51], general functional summaries [6], persistent entropy [4], and the Euler Characteristic Curve [50].

Of immediate importance to this paper are persistence landscapes, persistent entropy, and the Euler Characteristic Curve. Persistence landscapes provide a stable functional representation of a diagram by mapping the diagram to an element in L^2 . Persistent entropy, which defines an entropy derived from information theory, provides a stable summary of persistence diagrams. The Euler Characteristic Curve has been studied and used before the theory of persistent homology was developed. For example it has been used in the area of random fields [2]. The vectorization method that we introduce in this paper, called persistence curves, is a general framework from which we find that each of these examples above are a special case of or can easily be derived. In creating a summary method for persistence diagrams, one wishes for the summary to have a few important qualities. Qualities of a good vectorization method are neatly outlined in [1] and we list them here:

- Quality 1: The output of the representation is a vector in \mathbb{R}^n ;
- Quality 2: The representation is stable with respect to the input noise;
- Quality 3: The representation is efficient to compute;
- Quality 4: The representation maintains an interpretable connection to the original persistence diagram;
- Quality 5: The representation allows one to adjust the relative importance of points in different regions of the persistence diagram.

We will show throughout this paper that our proposed framework can generate vectorizations that possess several of these qualities. In the interest of space, we do not discuss computational efficiency in the main text. This information

appears in Appendix B. In addition to these qualities, one would want to validate the usefulness of the representation. To do this, we test the ability of persistence curves to inform texture classification.

Texture classification is a field within computer vision. Exhibitions of its usefulness are far reaching and can be found in several scientific areas such as image processing, material science [10], geology [48], brain disease [29], thyroid nodules [31], and also in TDA [16, 27, 35, 49]. The outline of this paper follows. In Section 2 we provide necessary background from the fields of TDA and image processing as it relates to this paper. Specifically, we formally define images as functions and relate them to topological objects known as cubical sets. We then briefly discuss the homology of cubical sets before defining persistent homology, persistence diagrams, and the discussing the stability of persistence diagrams. In Section 3, we propose our general framework, called the *persistence curve* (PC), for vectorizing persistence diagrams. We show that a number of well known vectorization methods can be realized as special cases of or derived from this framework. The framework itself depends on persistence diagrams and not the choice of underlying homology theory, hence persistence curves are applicable anytime persistence diagrams arise. We describe how we can use this framework to generate vectorizations that carry interpretable information about the persistence diagram and hence the underlying space from which the diagram is built. Several new vectorizations are proposed in this work as shown in Table 1. Finally, we prove a general bound on persistence curves as they relate to the distance between persistence diagrams.

We validate the usefulness of this framework in Section 4 when we apply persistence curves to the texture classification. In particular, we consider four popular texture databases: Outex [44], UIUCTex [46], KTH Texture under varying illumination, pose, and scale 2b (KTH-TIPS2b) [28], and the Flickr Material Database (FMD) [54]. We compare the performance of various persistence curves with other TDA methods showing that our method outperforms the others and provide empirical evidence of the computational efficiency of these curves. To aid reproducibility of our results, we've released a Python 3 package [33] that allows users to easily compute and create persistence curves. We conclude this work in Section 5 by presenting many possible avenues for the advancement of persistence curves.

2 Background

The main application involves texture classification for which we need to take images and turn them into topological objects suitable for our framework. This section focuses on developing the necessary background to understand this transformation. We begin by discussing images in a formal manner and then we give insight into how we assign topological spaces to them. We then briefly discuss homology before giving a light introduction to persistent homology, which gives us a way to summarize topological information in grayscale images. Though this section will deal specifically with images (hence cubical homology), neither

persistent homology nor persistence curves are restricted to this situation. For a more detailed discussion on homology and persistent homology, see e.g. [30] for cubical homology and [22] for persistent homology.

2.1 Binary and Grayscale Images

An **8-bit** $m \times n$ **grayscale image** is a function

$$I : \{0, 1, \dots, m-1\} \times \{0, 1, \dots, n-1\} \rightarrow \{0, 1, \dots, 255\}.$$

We treat an RGB color image as a triplet of gray-scale images. The pair (i, j) in the domain of I is called a **pixel** and its image under I , $I(i, j)$ is called a **pixel value**. We visualize images by using squares to represent pixels and color to represent the pixel values. For an 8-bit grayscale image, the pixel value indicates the shade of gray with 0 being black and 255 being white.

A **binary image** is one whose pixels only have two possible values. One may view a binary image as an image whose codomain is the set $\{0, 1\}$. For visualization, we associate 0 with the color black and 1 for white. We can describe a binary image I entirely by its support, which we denote as $K = \{(i, j) \mid I(i, j) = 1\}$. Then to a binary image, we can associate a union of unit squares $X = \bigcup_{(i,j) \in K} [i, i+1] \times [j, j+1]$. This kind of set is called a **cubical set**. More details of cubical sets appear in [30].

For an $n \times m$ grayscale image $I(i, j)$ and integer t , let $K_t = \{(i, j) \mid I(i, j) \leq t\}$. Let χ_A be the indicator function of a set A , i.e. $\chi_A(t) = 1$ if $t \in A$ and $\chi_A(t) = 0$ otherwise. We can construct a binary image by **thresholding** I at t using the function $I_t(i, j) = \chi_{K_t}(i, j)$. Notice that if $t \leq t'$ then $I_t(i, j) \leq I_{t'}(i, j)$, or equivalently, $K_t \subset K_{t'}$. For an 8-bit grayscale image, a **threshold decomposition** is an increasing sequence of binary images obtained by thresholding. In this paper, we use the decomposition $\{I_t\}_{t=0}^{255}$. Finally, we note that if X_t denotes the cubical set associated to I_t , then $X_t \subset X_{t'}$. Such a nested subset relation of topological spaces is known as **filtration**.

2.2 Persistent Homology

Homology is a classic subject in mathematics. It provides a discrete object as a descriptor of a topological space that is invariant under continuous deformations. This means that the homology of a space gives us useful information about its topological structure. Informally, the k -th homology group $H_k(X)$ of a space X is often used to count the **k -th Betti** numbers, i.e. the number of k -dimensional holes of X . For example in the case of binary images $H_0(X)$ counts the connected components (clusters of white pixels) and $H_1(X)$ counts the holes (clusters of black pixels surrounded by white pixels). The definition of cubical sets (unions of closed intervals) shows that connectivity in cubical homology is be equivalent to 4-connected neighborhood in the classic field of the connected-component labeling.

Figure 1(a) shows an example of a binary image that has 4 disjoint white regions, and hence, the 0-th level Betti number is 4, i.e. $\beta_0 = 4$. Moreover, since one



(a) $\beta_0(X) = 4$
 $\beta_1(X) = 1$.

(b) $\beta_0(X^c) = 3$
 $\beta_1(X^c) = 3$

Figure 1: X is the cubical set (union of unit squares of white pixels) of the binary image. An illustration of Betti numbers of a binary image and the boundary effect.

black region is enclosed completely by a white region (upper right circle in Figure 1(a), the first level Betti number is 1, i.e. $\beta_1 = 1$. Notice that the bottom left white region in Figure 1(a) looks like it might enclose another hole. However, since the white region does not wrap completely around the black region, it does not count towards β_1 . We see then that the boundary of the images plays an important role in counting Betti numbers. We refer to this as the **boundary effect**. In an attempt to account for the boundary effect, one may take the complement of the binary image (interchanging the colors) as shown in Figure 1(b). Intuitively, one may think that counting components in the complement image is the same as counting the holes in the original image. However, this is not the case as shown in Figure 1(b) that the Betti numbers of the complement image are $\beta_0 = 3$, and $\beta_1 = 3$. Together, the image and its complement lead us to an estimate of the true topological nature of the image. At this point, we can describe a binary image in terms of topology and we associate binary images to grayscale images. To extend the concept of Betti numbers to a grayscale image, we use persistent homology, a powerful tool from the field of computational topology. The origins begin with the size functions [25, 26] and is first formally defined in [23].

A **filtration** of a space X is an increasing sequence of spaces $\emptyset = X_0 \subset X_1 \subset \dots \subset X_n = X$. From the previous discussion, one may obtain homology groups for each X_i . Because of the subset relations, persistent homology allows us to track the changes of homology groups. We can equivalently view filtrations via a **filtering function** on the power set 2^X of X , $f : 2^X \rightarrow \mathbb{N}$ where $f^{-1}(t) \subset X$ is a subspace for all $m \in \mathbb{N}$, $f^{-1}(t) \subset f^{-1}(s)$ if $s \geq t$, and there is some $n \in \mathbb{N}$ for which $f^{-1}(n) = X$. The inclusion $X_t \subset X_s$ induces a map $g_{t,s}^k : H_k(X_t) \rightarrow H_k(X_s)$ between the homology groups.

We say a homology class α is **born** at b if we have $\alpha \in H_k(X_b)$ and $\alpha \notin \text{im } g_{b-1,b}^k$. We say that α born at b **dies** at d , $d \geq b$ if $g_{b,d-1}^k(\alpha) \notin \text{im } g_{b-1,d-1}^k$, but $g_{b,d}^k(\alpha) \in \text{im } g_{b-1,d}^k$, i.e. if it merges with a previous class. The ranks $\beta_{b,d}^k = \text{rank } \text{im } g_{b,d}^k$ for $d \geq b$ form the **persistent Betti numbers** of the filtration. These persistent Betti numbers count the number of classes that were born at or before b and are

still alive at d . Inclusion-exclusion allows us to count exactly the number $\mu_{b,d}^k$ of classes born at b and die at d by $\mu_{b,d}^k = \beta_{b,d-1}^k - \beta_{b-1,d-1}^k + \beta_{b-1,d}^k - \beta_{b,d}^k$. We may now define our topological summary. The **k -th persistence diagram**, or just **diagram**, $\mathcal{P}_k(f)$ associated to the filtering function f of a space X is a multi-set, that is a set of points with multiplicity, of birth-death pairs (b, d) with multiplicity $\mu_{b,d}^k$ along with the diagonal points (b, b) each with infinite multiplicity. To shorten notation, we will often represent persistence diagrams with the letter D .

For a grayscale image I we consider the cubical sets X_t associated to the binary threshold images I_t . We associate to I the filtration $X_0 \subset X_1 \subset \dots \subset X_{255}$. Hence, for any gray-scale image, we can obtain representative persistence diagrams. As these are 2D images, the only non-trivial diagrams are those from 0-th and 1-st dimension.

Let \mathcal{D} represent the set of all possible persistence diagrams that have finitely many off-diagonal points. An important property that \mathcal{D} possesses is so-called the stability theorem. The stability theorem for persistence diagrams, which first appeared in [18], states that if f_1, f_2 are filtering functions with certain regularity then

$$W_\infty(\mathcal{P}_k(f_1), \mathcal{P}_k(f_2)) \leq \|f_1 - f_2\|_\infty,$$

where $W_\infty(\mathcal{P}_k(f_1), \mathcal{P}_k(f_2))$ is known as the **Wasserstein ∞ -metric**, or **bottleneck distance** defined as

$$W_\infty(C, D) = \inf_{\substack{\text{bijections} \\ \eta: C \rightarrow D}} \sup_{x \in C} \|x - \eta(x)\|,$$

where $C, D \in \mathcal{D}$.

Summaries of persistence diagrams can be thought as a transformation from \mathcal{D} to a Hilbert space. As mentioned in Quality 2 in Section 1, it is desired to have a stability theorem for summaries of persistence diagrams. In the next section, we introduce our main PC framework, and establish a general bound that may lead to a stability theorem.

3 Persistence Curves and Stability

Persistence diagrams encode topological information of data sets. However, applying machine learning algorithms directly on the space of diagrams proves difficult. Our proposed framework called persistence curves gives us a way to further summarize persistence diagrams in a form that is compatible with machine learning and still retains some topological information about the space. This framework is inspired by the Fundamental Lemma of Persistent Homology (FLPH) [22, p. 118] stated below:

Fundamental Lemma of Persistent Homology. *Let $D_k = \mathcal{P}(f)$ be a diagram with respect to the filtering function f . Then*

$$\beta_k(f^{-1}(t)) = \sum_{i \leq t} \sum_{j > t} \mu_{a_i, a_j}^k. \quad (1)$$

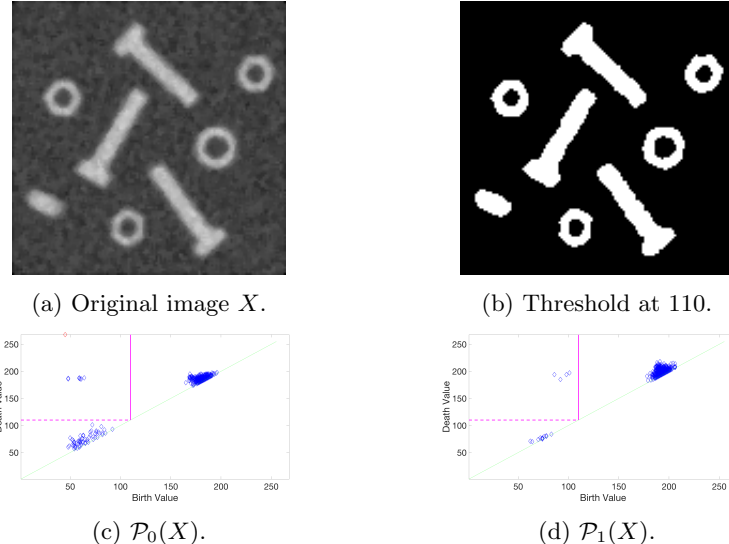


Figure 2: A toy example of persistence diagrams of a grayscale image. (a) By visual inspection, one expects the Betti numbers are $(8, 4)$. (b) Binary image is obtained from thresholding the X at 110. Betti number of this binary image are $(8, 4)$. (c)-(d) Persistence diagrams of X . The rectangular boxes enclosed by the pink dotted ($d > 110$) and solid line ($b \leq 110$) are the fundamental boxes $F_{110} = \{(b, d) \mid b \leq 110, d > 110\}$. $\beta_0(X_{110}) = 8$ and $\beta_1(X_{110}) = 4$.

This lemma states that the k -th Betti number of the space at filtration value t can be found by counting the points of the persistence diagram (with multiplicity) inside the **fundamental box** defined as

$$F_t = \{(b, d) \mid b \leq t, d > t\}. \quad (2)$$

Figure 2(c)-(d) shows the 0 and 1 dimensional persistence diagrams as well as an illustration of F_t .

We remark on methods for handling infinite generators whose death values is by convention ∞ . If there is a global maximum finite death value for the space, one may set all infinite death values to this maximum. Since images have a maximum possible finite death of 255, we opt to set the death value of infinite generators to this maximum. Another option would be to neglect infinite generators.

3.1 Persistence Curve Framework

Persistence curves use (2) to generate curves from persistence diagrams. Let \mathcal{D} be the set of all persistence diagrams, \mathcal{F} be the set of all functions $\psi : \mathcal{D} \times \mathbb{R}^3 \rightarrow \mathbb{R}$ with $\psi(D; b, b, t) = 0$ for all $(b, b) \in D$ and $D \in \mathcal{D}$. To ease the notation, we refer to $\psi(D; b, d, t)$ as $\psi(b, d, t)$ when D is understood. Moreover, when ψ does not depend on t , we write $\psi(b, d)$. Let \mathcal{T} be the set of **summary statistics** or operators on multi-sets (more precisely, any $T \in \mathcal{T}$ is a map that takes a multi-set into a scalar). Finally let \mathcal{R} represent the set of functions on \mathbb{R} .

Definition 1. We define a map $P : \mathcal{D} \times \mathcal{F} \times \mathcal{T} \rightarrow \mathcal{R}$ where

$$P(D, \psi, T)(t) := T(\psi(F_t, t)), \quad t \in \mathbb{R}.$$

The function $P(D, \psi, T)$ is called a **persistence curve** on D with respect to ψ and T .

Definition 1 is in a general format. If T does not depend on the cardinality of the set (e.g. if T is the max or sum operator), then the persistence curve $P(D, \psi, T)$ can be written in terms of indicator functions:

$$\begin{aligned} P(D, \psi, T) &= T(\{\psi(F_t, t)\}) = T_{(b,d) \in F_t} \{\psi(b, d, t)\} \\ &= T_{(b,d) \in D} \{\psi(b, d, t) \chi_{[b,d]}(t)\}. \end{aligned} \quad (3)$$

In the examples below we offer both reformulations of curves that have been proposed by prior works into the persistence curve framework as well as several new curves based on common persistence diagram statistics.

Example 1. Let $\mathbf{1}(x, y, t) = 1$ if $x \neq y$ and 0 otherwise. Let Σ be the summation operator. By Definition 1, we have

$$P(D, \mathbf{1}, \Sigma)(t) = \sum(\{\mathbf{1}(D; b, d, t) \mid b \leq t, d > t\}) = \beta(t).$$

This curve is the **Betti curve**, which has been described in other works [51], [3]. Furthermore, if $D_0, D_1, \dots, D_k, \dots$ are the k -dimensional diagrams associated

to a filtering function f , then the **Euler Characteristic** of the space X_t corresponding to a threshold t can also be expressed as a sum persistence curves evaluated at t . That is,

$$EC(X_t) := EC(t) = \sum_{i=0}^{\infty} (-1)^i \beta_i(t) = \sum_{i=0}^{\infty} (-1)^i P(D_i, \mathbf{1}, \Sigma)(t).$$

The **Euler Characteristic Curve** with respect to the filtering function f refers to the function

$$ECC(f) \equiv \sum_{i=0}^{\infty} (-1)^i P(D_i, \mathbf{1}, \Sigma).$$

We use the next example to illustrate explicitly how to calculate a persistence curve.

Example 2. Let $\psi(b, d, t) = d - b$ and $T = \Sigma$. Then by (3), $\mathbf{I}(D, t) := P(D, \psi, \Sigma) = \sum(\{d - b \mid b \leq t, d > t\})$, which we will refer as the lifespan curve.

Suppose $D = \{(1, 2), (2, 4), (2, 4), (3, 5), (1, 5)\}$. Then, by (3), it is straightforward to obtain that $\mathbf{I}(D, t) = \chi_{[1,2)}(t) + 2\chi_{[2,4)}(t) + 2\chi_{[2,4)}(t) + 2\chi_{[3,5)}(t) + 4\chi_{[1,5)}(t)$.

The meaning of this curve is that in addition to the Betti number, it also attaches the lifespan information. It can be seen as a topological intensity function. To the best of authors' knowledge, this curve is first appeared in this work.

The following are examples of vectorizations that have been independently studied by different groups, but can be realized in the framework of persistence curves.

Example 3. The PD Thresholding method [17] was developed as an optimal thresholding method in image processing based on persistence diagrams. The main idea is to define an objective function, and the optimal threshold will be chosen as the maximum of the objective function. One major component of the objective function in [17] is $O(t) = \frac{1}{\#F_t} \sum_{(b,d) \in F_t} (d - t)(t - b)$. The function $O(t)$ can be viewed as a persistence curve if one lets $\psi = (d - t)(t - b)$ and T be the average operator.

The following example can be found in [4], where the concept of entropy introduced to TDA.

Example 4. A summary function based on persistent entropy was defined as: $S(D)(t) = - \sum w(t) \frac{d-b}{L} \log(\frac{d-b}{L})$, where $L = \sum_{(b,d) \in D} (d - b)$ and $w(t) = 1$ if $b \leq t \leq d$ and $w(t) = 0$ otherwise. Let $\psi = -\frac{d-b}{L} \log \frac{d-b}{L}$, and $T = \Sigma$. We see that $E(D) := P(D, \psi, T)$ is similar to $S(D)$. In fact, due to the exclusion of the death value in the interval we have $0 \leq E(D) \leq S(D)$. Hence, $E(D)$ enjoys the same stability as $S(D)$, proven in [4].

In this last example, we also recognize persistence landscapes, a well-known diagram summary, as a special case of persistence curves.

Example 5. Let $\max_k(S)$ represent the k -th largest number of a set S . Given a persistence diagram D , define

$$l_{(b,d)}(t) = \begin{cases} 0 & \text{if } t \notin (b, d) \\ t - b & \text{if } t \in (b, \frac{b+d}{2}] \\ d - t & \text{if } t \in (\frac{b+d}{2}, d) \end{cases}.$$

Then the k -th Persistence Landscape [8] is defined by $\lambda_k(t) = \max_k\{l_{(b,d)}(t) \mid (b, d) \in D\}$. One can verify that $l_{(b,d)}(t) = \min\{t - b, d - t\}$. Thus, if $\psi(b, d, t) = \min\{t - b, d - t\}$ and $T = \max_k$, then $P(D, \psi, T) \equiv \lambda_k$.

We have shown that persistence curves provides a general framework for summarizing diagrams and that many existing summaries fall under the framework. Moreover, we propose several new summaries that we display in Table 1. By choosing ψ to be a function that carries sensible information about the diagram (hence the underlying space) we produce a persistence curve that does the same. For instance, the midlife quantity has been used in recent work, such as persistence landscapes [8] and persistence images [1] to serve as a linear transformations and to serve as classifiers [17]. The multiplicative life quantity has been studied in the field of random complexes [7]. As mentioned before, the life-entropy persistence curve actually appears as the entropy summary function in a recent work [4]. Motivated by this work, **mle**, **mule** are new entropy-like functions using the multiplicative life and midlife statistics. At this point, it should be clear that one could follow the framework to create new summaries of persistence diagrams.

3.2 A General Bound for PCs

In this subsection, we analyze the properties of persistence curves. The main focus will be on how changes in persistence diagrams affect persistence curves. Specifically, given two persistence diagrams $C, D \in \mathcal{D}$ and for fixed ψ and T , what is the difference between $P(C, \psi, T)$ and $P(D, \psi, T)$? Since PC is such a general framework, the stability analysis in this work focuses on the summation operator, i.e. $T = \Sigma$. Before our analysis, we will set up some notation and conventions. Let $C, D \in \mathcal{D}$. Let n represent the maximum between the number of off diagonal points in each diagram and note that n is finite. We assume the optimal matching under the bottleneck distance of these diagrams is known and we index the points of each diagram $\{(b_i^D, d_i^D)\}_{i=1}^n$ and $\{(b_i^C, d_i^C)\}_{i=1}^n$ so that points with matching indices are paired under the optimal matching. Other notations are summarized in Table 2. The first estimate is the key step towards to the general bound.

Lemma 1. *Let $h(t) = |\psi_1(t)\chi_{[b_1, d_1]}(t) - \psi_1(t)\chi_{[b_1, d_1]}(t)|$, where $b_1 \leq d_1$ and $b_2 \leq d_2$. Suppose that $\psi_i : [b_i, d_i] \rightarrow \mathbb{R}$ for $i = 1, 2$, respectively, are continuous.*

Name	Notation	$\psi(b, d, t)$	T
<i>Existing PCs</i>			
Betti number	β	1	sum
Life Entropy [4]	\mathbf{le}	$-\frac{d-b}{\sum(d-b)} \log \frac{d-b}{\sum(d-b)}$	sum
PD Thresholding [17]	O	$(d-t)(t-b)$	avg
k -th Landscape [8]	λ_k	$\min\{t-b, d-t\}$	\max_k
<i>PCs proposed in this work</i>			
Normalized Betti	\mathbf{sB}	$\frac{1}{n}$	sum
Life	\mathbf{l}	$d-b$	sum
Normalized Life	\mathbf{sl}	$\frac{d-b}{\sum(d-b)}$	sum
Midlife	\mathbf{ml}	$(b+d)/2$	sum
Normalized Midlife	\mathbf{sml}	$(b+d)/\sum(d+b)$	sum
Midlife Entropy	\mathbf{mle}	$-\frac{d+b}{\sum(d+b)} \log \frac{d+b}{\sum(d+b)}$	sum
Multiplicative Life	\mathbf{mul}	d/b	sum
Normalized Mult. Life	\mathbf{smul}	$\frac{d/b}{\sum d/b}$	sum
Mult. Life Entropy	\mathbf{mule}	$-\frac{d/b}{\sum(d/b)} \log \frac{d/b}{\sum(d/b)}$	sum

Table 1: Examples of persistence curves. In the top panel, existing summaries are realized in the PC framework. In the bottom panel, new summaries are proposed in this work. One can easily create new summaries by altering ψ and T .

Notation	Description
\vee	max operator, i.e. $n_1 \vee n_2 = \max\{n_1, n_2\}$
\wedge	min operator, i.e. $n_1 \wedge n_2 = \min\{n_1, n_2\}$
n^D	number of off diagonal points in D
n	$n^C \vee n^D$
(b_i^D, d_i^D)	point in the diagram D , indexed by the optimal matching
L^D, L_∞^D	$\sum d_i^D - b_i^D, \max_i(d_i^D - b_i^D)$
$\kappa(\psi, C, D)$	$\sum_{i=1}^n \max_{t \in [b_i^C, d_i^C]} \psi(b_i^C, d_i^C, t) \vee \sum_{i=1}^n \max_{t \in [b_i^D, d_i^D]} \psi(b_i^D, d_i^D, t) $
$\delta(\psi, C, D)$	$\max_{\substack{1 \leq i \leq n \\ t \in [b_i^C, d_i^C] \cap [b_i^D, d_i^D]}} \psi(b_i^C, d_i^C, t) - \psi(b_i^D, d_i^D, t) $

Table 2: The notation here pertains to two given diagrams C and D enumerated in correspondence to the optimal matching for the bottleneck distance.

Denote by $M = \max_{t \in [b_1, d_1]} \psi_1(t) \vee \max_{t \in [b_2, d_2]} \psi_2(t)$. Then we have

$$\begin{aligned} \|h\|_1 &\leq 2M(|d_2 - d_1| \vee |b_2 - b_1|) \\ &\quad + [(d_1 - b_1) \wedge (d_2 - b_2)] \max_{t \in [b_1, d_1] \cap [b_2, d_2]} |\psi_1(t) - \psi_2(t)|. \end{aligned}$$

Proof. According to the all possible orders of b_1, b_2, d_1, d_2 , there are six cases in total to consider. By symmetry, it remains the following three cases to consider. Case 1: $b_1 \leq d_1 \leq b_2 \leq d_2$ and $[b_1, d_1] \cap [b_2, d_2] = \emptyset$. By elementary calculation and $d_1 \leq b_2$, we obtain

$$\begin{aligned} \|f\|_1 &= \int_{b_1}^{d_1} |\psi_1(t)| dt + \int_{b_2}^{d_2} |\psi_2(t)| dt \\ &\leq M[(d_1 - b_1) + (d_2 - b_2)] \leq 2M(|d_2 - d_1| \vee |b_2 - b_1|). \end{aligned}$$

Case 2: $b_1 \leq b_2 \leq d_1 \leq d_2$ and $[b_1, d_1] \cap [b_2, d_2] = [b_2, d_1]$. By direct calculation, we obtain

$$\begin{aligned} \|f\|_1 &= \int_{b_1}^{b_2} |\psi_1(t)| dt + \int_{b_2}^{d_1} |\psi_1(t) - \psi_2(t)| dt + \int_{d_1}^{d_2} |\psi_2(t)| dt \\ &\leq M(b_2 - b_1) + (d_1 - b_2) \max_{t \in [b_2, d_1]} |\psi_1(t) - \psi_2(t)| + M(d_2 - d_1) \\ &\leq 2M(|b_2 - b_1| \vee |d_2 - d_1|) \\ &\quad + (d_1 - b_2) \max_{t \in [b_1, d_1] \cap [b_2, d_2]} |\psi_1(t) - \psi_2(t)|. \end{aligned}$$

Also, since $b_1 \leq b_2$ and $d_1 \leq d_2$, then $d_1 - b_2 \leq (d_1 - b_1)$ and $d_1 - b_2 \leq (d_2 - b_2)$. Hence, $d_1 - b_2 \leq (d_1 - b_1) \wedge (d_2 - b_2)$. Therefore, we have

$$\begin{aligned}\|f\|_1 &\leq 2M(|b_2 - b_1| \vee |d_2 - d_1|) \\ &\quad + (d_1 - b_1) \wedge (d_2 - b_2) \max_{t \in [b_1, d_1] \cap [b_2, d_2]} |\psi_1(t) - \psi_2(t)|.\end{aligned}$$

Case 3: $b_1 \leq b_2 \leq d_2 \leq d_1$ and $[b_1, d_1] \cap [b_2, d_2] = [b_2, d_2]$. By a similar calculation to Case 2, we obtain

$$\begin{aligned}\|f\|_1 &= \int_{b_1}^{b_2} |\psi_1(t)| dt + \int_{b_2}^{d_2} |\psi_1(t) - \psi_2(t)| dt + \int_{d_2}^{d_1} |\psi_1(t)| dt \\ &\leq M(b_2 - b_1) + (d_2 - b_2) \max_{t \in [b_2, d_2]} |\psi_1(t) - \psi_2(t)| + M(d_1 - d_2) \\ &\leq 2M|b_2 - b_1| \vee |d_2 - d_1| + (d_2 - b_2) \max_{t \in [b_2, d_2]} |\psi_1(t) - \psi_2(t)|.\end{aligned}$$

Similarly, in this case, it is straightforward to observe that $(d_2 - b_2) \leq (d_1 - b_1) \wedge (d_2 - b_2)$. Hence, we obtain

$$\begin{aligned}\|f\|_1 &\leq 2M(|b_2 - b_1| \vee |d_2 - d_1|) + \\ &\quad (d_1 - b_1) \wedge (d_2 - b_2) \max_{t \in [b_1, d_1] \cap [b_2, d_2]} |\psi_1(t) - \psi_2(t)|.\end{aligned}$$

This completes the proof. \square

Lemma 1 is the essential estimate in proving the main result stated below.

Theorem 1. *Let $C, D \in \mathcal{D}$ and index them through the optimal bottleneck distance matching. Let T be the Σ operator. Suppose that $T(\emptyset) = 0$. We adopt the notations in Table 2. Let $\psi(C, \cdot)$ and $\psi(D, \cdot)$ be continuous functions. Then the following estimate holds*

$$\begin{aligned}\|P(C, \psi, \Sigma) - P(D, \psi, \Sigma)\|_1 &\leq 2\kappa(\psi, C, D)W_\infty(C, D) + \\ &\quad (L^C \wedge L^D)\delta(\psi, C, D).\end{aligned}\tag{4}$$

Proof. Take the difference

$$\begin{aligned}\|P(C, \psi, \Sigma) - P(D, \psi, \Sigma)\|_1 &= \left\| \sum_{i=1}^n (\psi(b_i^C, d_i^C) \chi_{[b_i^C, d_i^C]} - \psi(b_i^D, d_i^D) \chi_{[b_i^D, d_i^D]}) \right\|_1 \\ &\leq \sum_{i=1}^n \int |\psi(b_i^C, d_i^C, t) \chi_{[b_i^C, d_i^C]}(t) - \psi(b_i^D, d_i^D, t) \chi_{[b_i^D, d_i^D]}(t)| dt.\end{aligned}\tag{5}$$

By Lemma 1, each integral in (5) is dominated by

$$\begin{aligned}
& \int |\psi(b_i^C, d_i^C, t) \chi_{[b_i^C, d_i^C]}(t) - \psi(b_i^D, d_i^D, t) \chi_{[b_i^D, d_i^D]}(t)| \, dt \\
& \leq 2M_i(|b_i^C - b_i^D| \vee |d_i^C - d_i^D|) + \\
& \quad [(d_i^C - b_i^C) \wedge (d_i^D - b_i^D)] \times \\
& \quad \max_{t \in [b_i^C, d_i^C] \cap [b_i^D, d_i^D]} |\psi(b_i^C, d_i^C, t) - \psi(b_i^D, d_i^D, t)|, \tag{6}
\end{aligned}$$

where $M_i = \max_{t \in [b_i^C, d_i^C]} |\psi(b_i^C, d_i^C, t)| \vee \max_{t \in [b_i^D, d_i^D]} |\psi(b_i^D, d_i^D, t)|$. Observe that $\sum_{i=1}^n M_i \leq \kappa(\psi, C, D)$, and $\sum_{i=1}^n [(d_i^C - b_i^C) \wedge (d_i^D - b_i^D)] \leq L^C \wedge L^D$. Also, by our notation, $\max_{1 \leq i \leq n} \{|b_i^C - b_i^D| \vee |d_i^C - d_i^D|\} = W_\infty(C, D)$. Therefore, from (5) and (6), we obtain

$$\begin{aligned}
& \sum_{i=1}^n \int |\psi(b_i^C, d_i^C, t) \chi_{[b_i^C, d_i^C]}(t) - \psi(b_i^D, d_i^D, t) \chi_{[b_i^D, d_i^D]}(t)| \, dt \\
& \leq \sum_{i=1}^n [2M_i(|b_i^C - b_i^D| \vee |d_i^C - d_i^D|) + [(d_i^C - b_i^C) \wedge (d_i^D - b_i^D)]] \\
& \quad \max_{t \in [b_i^C, d_i^C] \cap [b_i^D, d_i^D]} |\psi(b_i^C, d_i^C, t) - \psi(b_i^D, d_i^D, t)| \\
& \leq 2\kappa(\psi, C, D)W_\infty(C, D) + (L^C \wedge L^D)\delta(\psi, C, D).
\end{aligned}$$

□

Theorem 1 provides a general bound on the difference of two persistence curves. The following examples illustrate (5) on specific PCs. Some bounds obtained from (5) imply stability and some do not. In the next subsections, we demonstrate how to apply Theorem 1 to curves that we proposed.

3.3 Betti number curve

We first consider the Betti number curve as defined in Example 1. In this case, since $\psi(b, d, t) = 1$, by direct calculation one may obtain $\kappa(\psi, C, D) = n$ and $\delta(\psi, C, D) = 1$ (recall that $\psi(b, b, t) = 0$ for all b). Therefore, by Theorem 1, the bound for the Betti number curves is

$$\|\beta(C, t) - \beta(D, t)\|_1 \leq 2nW_\infty(C, D) + L^C \wedge L^D. \tag{7}$$

This bound does not imply the stability, because as $n \rightarrow \infty$, $L^C \wedge L^D \rightarrow \infty$. Up to authors' best knowledge, although Betti numbers have been widely used in many applications, the error bound (7) is one of the first attempts on the analysis.

With a simple modification, the bound (7) can be improved. Let $\psi(D; b, d, t) = \frac{1}{n^D} \mathbf{1}$. We called this *normalized Betti number curve* $\beta^S(D, t) := P(D, \frac{1}{n^D} \mathbf{1}, \Sigma)$. By direct calculation, we obtain $\delta(\psi, C, D) = \frac{1}{n^D \wedge n^C}$ and $\kappa(\psi, C, D) = 1$. Thus,

$$\|\beta^S(C, t) - \beta^S(D, t)\|_1 \leq 2W_\infty(C, D) + \frac{1}{n^D \wedge n^C} (L^C \wedge L^D). \tag{8}$$

Although the bound (8) does not imply the stability, it shows that the bound for the normalized Betti curve is smaller than that of the Betti curve. For instance, suppose that maximum lifespan of each persistence diagram is uniformly bounded by M . Then the latter term in (8) becomes $\frac{1}{n^D \wedge n^C} (n^C \wedge n^D) M = M$.

3.4 Bounds on lifespan related curves

Consider the example defined in Example 2, where $\psi(b, d) = d - b$ and $T = \Sigma$. By direct calculation, one may obtain $\kappa(\psi, C, D) = \sum_{1 \leq i \leq n} (d_i^C - b_i^C) \vee \sum_{1 \leq i \leq n} (d_i^D - b_i^D) = L^C \vee L^D$ and $\delta(\psi, C, D) = \max_{1 \leq i \leq n} |(d_i^C - b_i^C) - (d_i^D - b_i^D)| \leq 2W_\infty(C, D)$.

Therefore, by Theorem 1 and that $L^C \vee L^D + L^C \wedge L^D = L^C + L^D$,

$$\|\mathbf{l}(C) - \mathbf{l}(D)\|_1 \leq 2(L^C + L^D)W_\infty(C, D). \quad (9)$$

This does not imply stability with respect to $W_\infty(C, D)$ because L^C (L^D) might change as n changes.

However, similar to the normalized Betti number curve, we consider the normalized version of the lifespan curve by letting $\psi(D; b, d, t) = \frac{d-b}{L^D}$ to obtain

$$\mathbf{sl} := P(C, \frac{d-b}{L^D}, \Sigma). \quad (10)$$

Then it is straightforward to verify that $\kappa(\frac{1}{L}(d-b), C, D) = \frac{L^C}{L^C} \vee \frac{L^D}{L^D} = 1$. In order to obtain the estimate of δ , we first consider

$$\begin{aligned} & \left| \frac{d_i^C - b_i^C}{L^C} - \frac{d_i^D - b_i^D}{L^D} \right| \\ & \leq (|l_i^C| \vee |l_i^D|) \cdot \left| \frac{1}{L^C} - \frac{1}{L^D} \right| + \left(\frac{1}{L^C} \vee \frac{1}{L^D} \right) \cdot |l_i^C - l_i^D| \\ & \leq \frac{|l_i^C| \vee |l_i^D|}{L^C L^D} \cdot |L^C - L^D| + \frac{1}{L^C \wedge L^D} 2W_\infty(C, D), \end{aligned}$$

and take the maximum over i to obtain

$$\begin{aligned} \delta\left(\frac{d-b}{L}, C, D\right) &= \max_{1 \leq i \leq n} \left| \frac{d_i^C - b_i^C}{L^C} - \frac{d_i^D - b_i^D}{L^D} \right| \\ &\leq \frac{(L_\infty^C \vee L_\infty^D)}{L^C L^D} \cdot |L^C - L^D| + \frac{1}{L^C \wedge L^D} 2W_\infty(C, D) \\ &\leq \frac{(L_\infty^C \vee L_\infty^D)}{L^C L^D} 2nW_\infty(C, D) + \frac{1}{L^C \wedge L^D} 2W_\infty(C, D) \\ &= \left[\frac{(L_\infty^C \vee L_\infty^D)}{L^C L^D} 2n + \frac{2}{L^C \wedge L^D} \right] W_\infty(C, D). \end{aligned} \quad (11)$$

Finally, by the above inequality and that $\frac{L^C \wedge L^D}{L^C L^D} = \frac{1}{L^C \vee L^D}$,

$$\begin{aligned}
& \| \mathbf{sl}(C) - \mathbf{sl}(D) \|_1 \\
& \leq 2\kappa(\psi, C, D)W_\infty(C, D) + (L^C \wedge L^D)\delta(\psi, C, D) \\
& \leq 2W_\infty(C, D) + \left[\frac{(L_\infty^C \vee L_\infty^D)}{L^C \vee L^D} 2n + 2 \right] W_\infty(C, D) \\
& = \left[\frac{L_\infty^C \vee L_\infty^D}{L^C \vee L^D} 2n + 4 \right] W_\infty(C, D).
\end{aligned} \tag{12}$$

The bound (12) is better than (9) because as n increases, the quantity $L^C \vee L^D$ increases as well. For instance, in the case the grayscale image, the smallest $l_i = 1$. If we further assume that there is a uniform lower and upper bound on $(d - b)$, then the normalized lifespan curve is stable with respect to the W_∞ . More precisely, if we assume $(d - b) \leq M$, and $d - b > m > 0$ for all $(b, d) \in D$, then (12) becomes

$$\left[\frac{L_\infty^C \vee L_\infty^D}{L^C \vee L^D} 2n + 4 \right] W_\infty(C, D) \leq [2\frac{M}{m} + 4] W_\infty(C, D). \tag{13}$$

We formalize the discussion of the normalized lifespan curve in Example 2 in the following result.

Corollary 1. (i) *Let the normalized lifespan curve \mathbf{sl} be defined as in (10). Then for all $C, D \in \mathcal{D}$,*

$$\| \mathbf{sl}(C) - \mathbf{sl}(D) \|_1 \leq \left[\frac{L_\infty^C \vee L_\infty^D}{L^C \vee L^D} 2n + 4 \right] W_\infty(C, D).$$

(ii) *Moreover, let M and m be some positive integers. Denote $\mathcal{D}_{M,m} := \{D \in \mathcal{D} \mid d - b \leq M, d - b > m, \forall (b, d) \in D\}$. Then for all $C, D \in \mathcal{D}_{M,m}$,*

$$\| \mathbf{sl}(C) - \mathbf{sl}(D) \|_1 \leq [2\frac{M}{m} + 4] W_\infty(C, D), \tag{14}$$

which means that \mathbf{sl} is stable with respect to W_∞ in $\mathcal{D}_{M,m}$.

The collection $\mathcal{D}_{M,m}$ is not empty. For instance, in the case of 8-bit digital images, the smallest (largest) possible lifespan is 1 (255, respectively).

By a similar argument, we could establish the result for the midlife curve. More precisely, consider

$$\mathbf{sml}(D, t) := P(D, \frac{u}{U}, \Sigma), \tag{15}$$

where $u = d + b$ and $U = \sum(d + b)$. It is straightforward to verify that $\max_{1 \leq i \leq n} |u_i^C - u_i^D| \leq 2W_\infty(C, D)$, $|U^C - U^D| \leq 2nW_\infty(C, D)$, and that $\frac{L^C \wedge L^D}{U^C \wedge U^D} < 1$. Thus $\kappa(\frac{u}{U}, C, D) \leq 1$ and $\delta(\frac{u}{U}, C, D) \leq \left[\frac{(U_\infty^C \vee U_\infty^D)}{U^C \wedge U^D} 2n + \frac{2}{U^C \wedge U^D} \right] W_\infty(C, D)$.

Corollary 2. (i) Let the normalized midlife curve \mathbf{sml} be defined as in (15). Then for all $C, D \in \mathcal{D}$,

$$\|\mathbf{sml}(C) - \mathbf{sml}(D)\|_1 \leq \left[\frac{U_\infty^C \vee U_\infty^D}{U^C \vee U^D} 2n + 4 \right] W_\infty(C, D).$$

(ii) Moreover, let M and m be some positive integers. Denote $\tilde{\mathcal{D}}_{M,m} := \{D \in \mathcal{D} \mid d + b \leq M, d + b > m, \forall (b, d) \in D\}$. Then for all $C, D \in \tilde{\mathcal{D}}_{M,m}$,

$$\|\mathbf{sml}(C) - \mathbf{sml}(D)\|_1 \leq [2 \frac{M}{m} + 4] W_\infty(C, D), \quad (16)$$

which means that \mathbf{sml} is stable with respect to W_∞ in $\tilde{\mathcal{D}}_{M,m}$.

Lastly, we consider $E(D)$ defined in Example 4 who also defined the relative error between diagrams C and D to be $r_\infty(C, D) = \frac{2nW_\infty(C, D)}{L^C \vee L^D}$. If we assume $r_\infty(C, D) \leq \frac{1}{4}$ then it can be verified that if $|x - y| \leq 2r_\infty(C, D)$, then $|x \log x - y \log y| \leq 2r_\infty(C, D) \log 2r_\infty(C, D)$. If $\psi(D; b, d, t) = -\frac{d-b}{L^D} \log \frac{d-b}{L^D}$. Then we find $\kappa(\psi, C, D) \leq \Psi^C \vee \Psi^D \leq \log n$ and $\delta(\psi, C, D) = 2 \frac{2nW_\infty(C, D)}{L^C \vee L^D} \log(2 \frac{2nW_\infty(C, D)}{L^C \vee L^D})$. This bound is exactly the same as that of [4].

We can generalize the life entropy curve by recognizing its general shape as $\psi(D; b, d, t) = -\frac{f(b, d)}{\sum f(b, d)} \log \frac{f(b, d)}{\sum f(b, d)}$. One such example of this generalized formula is the *midlife entropy curve* where we take $f(b, d) = b + d = u$. Let $U^C = \sum u^C$ and analogously for D . Notice that if $(b, d) \in \mathbb{R}_{\geq 0}^2$ for all $(b, d) \in C \cup D$, then $\frac{2nW_\infty(C, D)}{U^C \vee U^D} \leq \frac{2nW_\infty(C, D)}{L^C \vee L^D}$. In particular, if $r_\infty(C, D) \leq \frac{1}{4}$, we retrieve the following bound on the midlife entropy curve. If $\psi(D; b, d, t) = \psi(D; b, d) = -\frac{u}{U^D} \log \frac{m}{U^D}$, then we find $\kappa(\psi, C, D) = \Psi^C \vee \Psi^D$ and $\delta(\psi, C, D) = \frac{2nW_\infty(C, D)}{U^C \vee U^D} \log \frac{2nW_\infty(C, D)}{U^C \vee U^D}$.

3.5 Bounds on Persistence Landscapes

So far we have discussed persistence curves that use summation as the statistic. Presently, we discuss the persistence landscape that uses $\psi(b, d, t) = \min\{t - b, d - t\}$ and $T = \max$. It is important to note that the Theorem 1 does not apply in this case. However, using this framework, we could reproduce the stability result (Theorem 12 in [8]) of persistence landscapes by elementary computation, which states

$$\|P(C, \psi, \max) - P(D, \psi, \max)\|_\infty \leq W_\infty(C, D). \quad (17)$$

The main idea of this elementary proof is to establish a similar result to Lemma 1.

Lemma 2. Let $f(t) = |\psi_1(t)\chi_{[b_1, d_1]}(t) - \psi_2(t)\chi_{[b_2, d_2]}(t)|$, where $\psi_i(t) = \min\{t - b_i, d_i - t\}$ for $i = 1, 2$. Then

$$\|f\|_\infty \leq |d_2 - d_1| \vee |b_2 - b_1|. \quad (18)$$

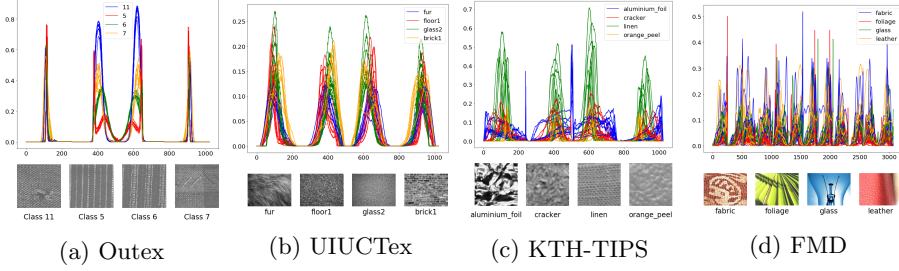


Figure 3: The Betti curves ($[\mathbf{ml}_0(I), \mathbf{ml}_1(I), \mathbf{ml}_0(I^C), \mathbf{ml}_1(I^C)]$) for each image I in 4 selected classes from the specified database.

Proof. Similar to the proof of Lemma 1, there are three cases to consider. In each case, by the fact that $\max_{t \in (b, d)} \min\{t - b, d - t\} = \frac{d-b}{2}$ when $t = \frac{b+d}{2}$, it is straightforward to obtain the estimate (18). For the sake of the completion, more details of the proof are included in the Appendix. \square

Thus, to prove (17), by Lemma 2 we obtain

$$\begin{aligned}
 & \|P(C, \psi, \max) - P(D, \psi, \max)\|_\infty \\
 &= \max_{1 \leq i \leq n} \left[\max_{t \in [b_i^C, d_i^C] \cup [b_i^D, d_i^D]} |\psi(b_i^C, d_i^C, t) \chi_{[b_i^C, d_i^C]}(t) \right. \\
 &\quad \left. - \psi(b_i^D, d_i^D, t) \chi_{[b_i^D, d_i^D]}(t)| \right] \\
 &\leq \max_{1 \leq i \leq n} |d_i^C - d_i^D| \vee |b_i^C - b_i^D| = W_\infty(C, D).
 \end{aligned}$$

It should be noted that we can obtain persistence landscapes for any level by taking $T = \max_k$ for the desired level k .

Persistence curves serve as a general framework that leads a family of vectorizations of persistence diagrams. We have shown a general stability result from which we can derive stability results for several specific curves. In the next section, we will test the usefulness of this framework in an application to texture classification.

4 Applications to texture analysis

In the previous sections, we developed persistence curve framework, demonstrated several examples as existing summaries, and proposing new ones. In this section, we will use persistence curves that are developed in Section 3 to study real datasets. In particular, we are interested in texture classifications. Texture analysis is a fundamental research area in computer vision. One challenge in the area is to find intrinsic characteristics, or quantitative representations of textures in order to perform classifications, or employ statistics. PCs can be served as intrinsic characteristics of the textures, and this section is devoted to demonstrating effectiveness of PCs and their usefulness in texture classification.

4.1 Descriptions of the data

We consider four publicly available texture databases and describe each of them below.

(i) **Outex (OT):** a database from the University of Oulu and consists of 15 test suites each with a different challenge [44]. We focus on the test suites 0, and 10. Test suite 0 contains 24 texture classes with 20 grayscale images of each class that are 128 by 128 in size. The test suite 0 is equipped with 100 preset 50-50 train/test splits. A score on the test suite 0 is the average accuracy over all 100 splits. Test suite 10 tests rotational invariance. In this suite there is a single train/test split of the 4320 images with the training set containing 1/9 of the images. A score on this test suite is a single accuracy score.

(ii) **UIUCTex (UIUC):** a collection of textures from University of Illinois Urbana-Champagne [34]. The dataset consists of 25 texture classes with 40 grayscale images of each texture. Each image is of size 640 by 480. Following the methods of [47], a score on this set is the average accuracy of 100 random 80/20 train/test splits.

(iii) **KTH-TIPS2b (KTH):** The KTH Textures under varying Illumination, Pose and Scale (TIPS) is a database containing 81 200 by 200 grayscale images for each of its 10 textures [28]. As the name suggests, each texture class contains images of different scales, rotations, and illuminations. A score on this set is the average accuracy of 100 random 80/20 train/test splits.

(iv) **FMD:** The Flickr Material Database contains 100 RGB images of sizes 512 by 384 for each of its 10 materials [54]. This database is the most challenging as it focuses more on material recognition rather than texture classification. That is, the classes contain images of many different objects at different scales that are of the same material (glass, leather, etc.) but may have widely different textures. A score on this set is the average accuracy of 100 random 80/20 train/test splits.

Some sample images from each dataset are shown in Figure 3.

4.2 Feature Vectors

The main idea in the classification is to use PCs to produce input vectors for machine learning algorithms. First, we use **Perseus** [42] to compute persistence diagrams. For each image I , we use the 0 and 1 dimensional diagrams $D_0(I), D_1(I)$. We also consider the complement of the image. More precisely, consider the image $I^C(i, j) := 255 - I(i, j)$. Topologically speaking, taking both I and I^C into account yields the same result. However, due to the boundary effect, taking I into account provides an estimation of the true topological nature and the complement of I provides a complementary estimation. We refer the reader back to Figure 1. Hence, for each gray-scale image, we have four corresponding diagrams, $D_0(I), D_1(I), D_0(I^C), D_1(I^C)$. Finally, for an RGB image, we consider each channel (i.e. the red, green, or blue channel) as a gray-scale image. Hence, each RGB image yields 12 corresponding diagrams.

Since the images we consider are 8-bit grayscale images, their pixel values are

integers from 0 to 255. Therefore, the persistence curves evaluated at those integers are enough to represent the curves. More precisely, in the case of 8-bit grayscale images, the set $\{P(D, \psi, T)(k)\}_{k=0}^{255}$ contains all information about $P(D, \psi, T)$. Therefore, each $P(D, \psi, T)$ is a vector of dimension 256.

Secondly, we concatenate the persistence curve vectors and these vectors serve as feature vectors. Each feature vector for a grayscale (color) image is a vector of dimension 256×4 ($256 \times 4 \times 3$). E and S are sets of feature vectors consisting of $E = [\mathbf{le}, \mathbf{mle}, \mathbf{mule}]$ and $S = [\mathbf{sl}, \mathbf{sml}, \mathbf{smul}]$, respectively. Thus, E for a grayscale (color) image is a vector of dimension $256 \times 4 \times 3$ ($256 \times 4 \times 3 \times 3$). From the definition, we see that Persistence Curves extracts local information from the persistence diagrams. In the interest of also extracting global information, we include persistence statistics [17]. Persistence statistics summarize diagrams by assigning them to a single number. For each diagram D , we consider two sets of numbers: $\{(b+d)/2 \mid (b, d) \in D\}$ and $\{d-b \mid (b, d) \in D\}$. On each of these sets we calculate the following 9 statistical measurements: mean, median, standard deviation, skewness, kurtosis, the 10th, 25th, 75th, 90th percentiles. For an image I , PS will represent the vector composed of the above statistics for $D_0(I), D_1(I), D_0(I^C), D_1(I^C)$.

4.3 Models

In order to illustrate the effectiveness of PCs, we keep our classification pipeline and model simple. Schematically speaking, for a given image I , (1) we consider both I and its complement I^C ; (2) we calculate persistence diagrams $D(I)$, $D(I^C)$ by `perseus`; (3) we compute discretized persistence curves from $D(I)$ and $D(I^C)$ by using the sequence $\{0, 1, \dots, 255\}$; (4) we feed the resulting vectors into machine learning algorithms. If I is a color image, then we consider each channel independently and apply each the above pipeline to each channel.

The main machine learning algorithms we use in this article are random forest (RF) with 500 estimators and Support Vector Machines with a linear kernel and one-vs-rest multi-class strategy. For reproducibility, both are from the Python package sci-kit learn.

4.4 Texture Classification

Table 3 shows the performances of various persistence curves, and other TDA methods from the literature on the 4 databases. We reiterate that we did not alter the original image in any way other than considering the image and its complement. We also did not tune the RF nor SVM in an effort to check the performance of persistence curves on raw images. Table 3 contains the highlight of our performances. We include much more experiments and their performance in the Appendix, specifically Table 5. We discuss the results below.

Observe the β curves, which do not take advantage of persistence diagrams, already perform well on these four databases. This may suggest that topological invariants are well-suited for the texture representations. The performances of l , however, are on par with those of β . One explanation may be that total

life span is correlated with the number of generators if the number of short life generators dominates. When considering the normalized life span curves \mathbf{sl} , the performances improve considerably from those of β (e.g. from 87.3% to 92.9% in the case of UIUC). The best performance for using only persistence curves is the concatenation of normalized curves, S . We also observe that the performances of entropy curves are similar to those of normalized curves as shown in Table 5 in Appendix; however, normalized curves are computationally less complex, and have a better stability bound. Thus, we believe that normalized curves would be the preferable option.

We turn our focus to compare the performances of our methods with those of other TDA methods: Sparse-TDA developed by [27] (66%), kernel-TDA by [49] (69.2%), CLBP-SMC by [35] (87.5%), k_{PSS} by [11] (98.8%), and persistence path by [16] (97.8%). These methods were all applied to OT0. Note that Sparse-TDA, kernel-TDA, CLBP-SMC, k_{PSS} are all kernel based methods. In particular, k_{PSS} seems to perform best out of the TDA methods on OT0. We see all persistence curves perform consistently on a level similar to these high performing TDA methods ($> 96\%$), particularly $E + PS + RF$ achieving a score of 98.5. The Benchmark model for OT0 was given by the Gabor filtering [24]. It is on UIUCTex and KTH that we begin to see the effects of stability on the curves. Both of these databases are more complex than Outex and it shows in the performance reduction of the Betti and lifespan curves. The TDA method EKFC+LMNN is a vectorization method that computes a descriptor based on the topology of a klein bottle, then combines this set of vectors with a metric learned through Large Margin Nearest Neighbors [47]. We find that on UIUC, the models $\mathbf{sl} + RF$, $S + RF$, $S + PS + RF$, and $E + S + PS + SVM$ outperform the klein bottle method; on KTH, the $E + S + PS + SVM$ model outperforms the klein bottle method.

Among these 4 databases, the FMD is the most challenging one. Within each class these materials will have different colors and even different textures. The scores shown in 3 is comparable to those in [37] (which is 44.6%). We see the $E + S + PS + SVM$ method falter a little bit here while the $S + PS + RF$ method performs best out of the persistence curves. The reason for this is likely due to the fact that E and S contains local information while PS contains global information. In Support Vector Machines each tiny change in global features is treated the same as a tiny change in local features since all inputs are considered vectors in Euclidean space. The Random Forest algorithm makes no such assumption and attempts to discern which differences are more important. Finally, we also compare our performances with state-of-arts ones reported in the survey paper [38]. We observe that our performances fall a little behind the state-of-arts, specifically 98.5% v.s. 99.5% in OT0, 97.7% v.s. 100% in OT10, 99.0% v.s. 93.5% in UIUC, 95.9% v.s. 99.4% in KTH, and 43.6% v.s. 59.8% in FMD. Our method does not involve parameter tuning. Also, since the main focus of this work is to demonstrate usefulness and effectiveness of PCs, we do not optimize our procedure. There are many directions that may improve our performances. For instance, we consider Euclidean distance for the persistence curves, and perhaps there are better metrics for the distance between curves.

Our Methods	OT0	OT10	UIUC	KTH	FMD
β + RF	97.3	96.0	87.1	90.5	37.2
1 + RF	95.8	94.5	87.3	90.5	35.8
sl + RF	96.8	94.7	92.9	93.8	40.2
S + RF	98.3	97.2	93.5	93.1	41.8
$S + PS$ + RF	98.5	97.7	93.5	94.4	43.6
$E + S + PS$ + SVM	95.9	96.1	92.2	95.9	33.7
Benchmarks* [38]	99.5**	100.	99.0	99.4	59.8
Other TDA models					
sparse-TDA [27]	66.0	-	-	-	-
Kernel-TDA [49]	69.2	-	-	-	-
CLBP-SMC [35]	87.5	-	-	-	-
k_{PSS} [11]	98.8	-	-	-	-
Persistence Paths [16]	97.8	-	-	-	-
EKFC+LMNN [47]	-	-	91.2	94.8	-

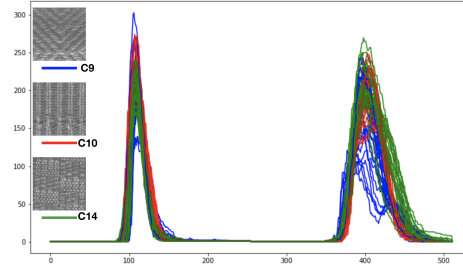
Table 3: Performance on Outex, UIUCTex, KTH-TIPS, and FMD. Highlighted rows signify the best performance in the column, bold text indicates the best of the TDA methods, italicics indicate the best PC model. *Benchmarks were reported in [38] with different methods based on traditional bag of words based texture representation; the results for CNN based representations are not shown here. **Since the score of OT0 is not available in [38], we reported the score from the work [24].

There are also several other tools we could use to better understand PCs, such as developing a method of statistical curve selection or trying other MLAs. We've simply seen so far that persistence curves form a useful, topological representation of the underlying set that has a meaningful interpretation.

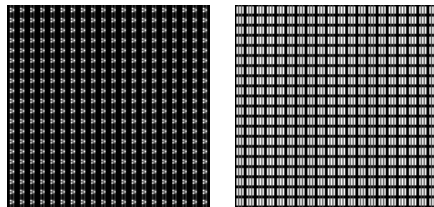
4.5 Efficiency, Limitation, and Robustness

The computational efficiency of persistence curves depends on the chosen curve ψ , the number of points in a given diagram $\#D$, and the number of mesh points (denoted by M) at which the curve is evaluated t . From the Definition 1, we observe that the complexity of computing PC is roughly linear in both threshold and number of generators. Numerical experiments confirmed the observation. Details of this experiments are included in Appendix B.

It is important to note that these persistence curves have some limitations. Because diagrams are not unique to a particular space, different textures may have similar persistence diagrams. This inverse problem is a challenging problem, and is a new research area in TDA [19, 43, 45]. To illustrate this, we manually generate two images as shown in Figure 4(b)-(c). To the human eye, these look like images of two different textures, but they actually produce the exact same persistence diagrams. While it is unlikely that real textures will produce ex-



(a) Misclassification on OT0.



(b)

(c)

Figure 4: (a) Most frequently misclassified classes (Class9, Class10, Class14) in OT0 and their corresponding Betti curves. (b)-(c) The two figures seem to have different textures, but they yield the same persistence diagrams (not shown).

actly the same diagram, it is possible for different textures to produce similar diagrams hence similar persistence curves. For example in Figure 4(a) we see 3 different classes of canvas textures in OT0. These 3 classes most often confused the classifiers. The rotational and size invariance of the topological descriptors play roles in this confusion as we see these textures have similar patterns in different sizes and orientations. In the future work, it would be interesting to investigate those textures with the same (or similar) persistence diagrams in order to fully understand the bottleneck of this method and hence, to improve it.

We end this section by discussing the experimental stability of curves. Table 4 shows the classification accuracies of the given curves after the images of KTH and OT0 have been altered by the given percentage of salt and pepper noise. There are two main observations. For one, the performances of normalized curves are better. Moreover, we see the more unstable curves like the Betti and lifespan curve lose performance more quickly than their more stable counterparts.

5 Generalization and Conclusion

Persistence curves provide a simple general framework from which we can generate models that are suitable for modern data analytics techniques and that

Database	Curve	0%	10%	20%	30%	40%
KTH	β +RF	90.5	86.4	84.2	80.3	79.2
KTH	β^S +RF	92.0	89.9	87.8	86.6	84.7
OT0	1+RF	95.8	81.9	83.6	85.3	84.3
OT0	sl+RF	96.8	93.4	92.9	91.6	90.8

Table 4: The effects of salt and pepper noise in the KTH and OT0 database on persistence curves.

retain the topological information contained in the persistence diagrams they are calculated from. These curves are compatible with machine learning algorithms, they can be stable, they are efficient to compute, and by choice of functions and statistics, one can alter the importance of points in different regions of the persistence diagrams. We have also shown that these curves create useful classifiers for texture analysis. The theory and experimentation presented here are by no means complete. We conclude this paper by listing below several potential directions for further investigation.

Questions.

- Q1 In Theorem 1, the operator T is fixed as Σ . . What conditions on the function ψ or the statistic T can lead to a more general and useful stability result?
- Q2 Several statistical properties, such as laws of large numbers, and stochastic convergence [9,13,14], of persistence landscapes has been established. Since persistence landscapes fall under the pc framework, it would be interesting to investigate general conditions on ψ and T so that the same properties hold.
- Q3 The Euler Characteristics Transform [55] was proved to be a sufficient statistic for distributions on the space of subsets of \mathbb{R}^d that can be written as simplicial complexes where $d = 2, 3$, and was applied to shape analysis. It would be interesting to generalize this concept to persistence curves.
- Q4 Is there a statistical framework to perform “curve selection” that will produce an optimal or near optimal set of curves for modeling?
- Q5 Could weighting be used to improve performance? In particular, is there a nice way to combine the local Persistence Curves with the global Persistent Statistics?

References

- [1] Henry Adams, Tegan Emerson, Michael Kirby, Rachel Neville, Chris Peterson, Patrick Shipman, Sofya Chepushtanova, Eric Hanson, Francis Motta,

and Lori Ziegelmeier. Persistence images: A stable vector representation of persistent homology. *The Journal of Machine Learning Research*, 18(1):218–252, 2017.

- [2] Robert J Adler. *The geometry of random fields*. SIAM, 2010.
- [3] N. Atienza, R. Gonzalez-Diaz, and M. Soriano-Trigueros. A new entropy based summary function for topological data analysis. *Electronic Notes in Discrete Mathematics*, 68:113 – 118, 2018. Discrete Mathematics Days 2018.
- [4] Nieves Atienza, Rocío González-Díaz, and M. Soriano-Trigueros. On the stability of persistent entropy and new summary functions for TDA. *CoRR*, abs/1803.08304, 2018.
- [5] Paul Bendich, James S Marron, Ezra Miller, Alex Pieloch, and Sean Skwerer. Persistent homology analysis of brain artery trees. *The annals of applied statistics*, 10(1):198, 2016.
- [6] Eric Berry, Yen-Chi Chen, Jessi Cisewski-Kehe, and Brittany Terese Fasy. Functional summaries of persistence diagrams. *arXiv preprint arXiv:1804.01618*, 2018.
- [7] Omer Bobrowski, Matthew Kahle, Primoz Skraba, et al. Maximally persistent cycles in random geometric complexes. *The Annals of Applied Probability*, 27(4):2032–2060, 2017.
- [8] Peter Bubenik. Statistical topological data analysis using persistence landscapes. *The Journal of Machine Learning Research*, 16(1):77–102, 2015.
- [9] Peter Bubenik. The persistence landscape and some of its properties. *arXiv preprint arXiv:1810.04963*, 2018.
- [10] H-J Bunge. *Texture analysis in materials science: mathematical methods*. Elsevier, 2013.
- [11] Mathieu Carrière, Marco Cuturi, and Steve Oudot. Sliced Wasserstein kernel for persistence diagrams. In Doina Precup and Yee Whye Teh, editors, *Proceedings of the 34th International Conference on Machine Learning*, volume 70 of *Proceedings of Machine Learning Research*, pages 664–673, International Convention Centre, Sydney, Australia, 06–11 Aug 2017. PMLR.
- [12] Corrie J Carstens and Kathy J Horadam. Persistent homology of collaboration networks. *Mathematical problems in engineering*, 2013, 2013.
- [13] Frédéric Chazal, Brittany Fasy, Fabrizio Lecci, Bertrand Michel, Alessandro Rinaldo, and Larry Wasserman. Subsampling methods for persistent homology. In *International Conference on Machine Learning*, pages 2143–2151, 2015.

- [14] Frédéric Chazal, Brittany Terese Fasy, Fabrizio Lecci, Alessandro Rinaldo, and Larry Wasserman. Stochastic convergence of persistence landscapes and silhouettes. In *Proceedings of the thirtieth annual symposium on Computational geometry*, page 474. ACM, 2014.
- [15] Yen-Chi Chen, Daren Wang, Alessandro Rinaldo, and Larry Wasserman. Statistical analysis of persistence intensity functions. *arXiv preprint arXiv:1510.02502*, 2015.
- [16] Ilya Chevyrev, Vidit Nanda, and Harald Oberhauser. Persistence paths and signature features in topological data analysis. *arXiv preprint arXiv:1806.00381*, 2018.
- [17] Yu-Min Chung and Sarah Day. Topological fidelity and image thresholding: A persistent homology approach. *Journal of Mathematical Imaging and Vision*, pages 1–13, 2018.
- [18] David Cohen-Steiner, Herbert Edelsbrunner, and John Harer. Stability of persistence diagrams. *Discrete & Computational Geometry*, 37(1):103–120, 2007.
- [19] Justin Curry. The fiber of the persistence map. *arXiv preprint arXiv:1706.06059*, 2017.
- [20] Vin De Silva, Robert Ghrist, et al. Coverage in sensor networks via persistent homology. *Algebraic & Geometric Topology*, 7(1):339–358, 2007.
- [21] Irene Donato, Matteo Gori, Marco Pettini, Giovanni Petri, Sarah De Nigris, Roberto Franzosi, and Francesco Vaccarino. Persistent homology analysis of phase transitions. *Physical Review E*, 93(5):052138, 2016.
- [22] H. Edelsbrunner and J. Harer. *Computational Topology: An Introduction*. Miscellaneous Books. American Mathematical Society, 2010.
- [23] Herbert Edelsbrunner, David Letscher, and Afra Zomorodian. Topological persistence and simplification. In *Proceedings 41st Annual Symposium on Foundations of Computer Science*, pages 454–463. IEEE, 2000.
- [24] Hans G Feichtinger and Thomas Strohmer. *Gabor analysis and algorithms: Theory and applications*. Springer Science & Business Media, 2012.
- [25] Massimo Ferri, Patrizio Frosini, Alberto Lovato, and Chiara Zambelli. Point selection: A new comparison scheme for size functions (with an application to monogram recognition). In *Asian Conference on Computer Vision*, pages 329–337. Springer, 1998.
- [26] Patrizio Frosini. Measuring shapes by size functions. In *Intelligent Robots and Computer Vision X: Algorithms and Techniques*, volume 1607, pages 122–134. International Society for Optics and Photonics, 1992.

- [27] Wei Guo, Krithika Manohar, Steven L Brunton, and Ashis G Banerjee. Sparse-tda: Sparse realization of topological data analysis for multi-way classification. *IEEE Transactions on Knowledge and Data Engineering*, 30(7):1403–1408, 2018.
- [28] Eric Hayman, Barbara Caputo, Mario Fritz, and Jan-Olof Eklundh. On the significance of real-world conditions for material classification. In *European conference on computer vision*, pages 253–266. Springer, 2004.
- [29] Maria Del C Valdés Hernández, Victor González-Castro, Francesca M. Chappell, Eleni Sakka, Stephen Makin, Paul A. Armitage, William H. Nailon, and Joanna M. Wardlaw. Application of texture analysis to study small vessel disease and bloodbrain barrier integrity. In *Front. Neurol.*, 2017.
- [30] T. Kaczynski, K. Mischaikow, and M. Mrozek. *Computational Homology*. Applied Mathematical Sciences. Springer New York, 2004.
- [31] Soo-Yeon Kim, Eun-Kyung Kim, Hee Jung Moon, Jung Hyun Yoon, and Jin Young Kwak. Application of texture analysis in the differential diagnosis of benign and malignant thyroid nodules: Comparison with gray-scale ultrasound and elastography. *AJR. American journal of roentgenology*, 205(3):W343–51, 2015.
- [32] Genki Kusano, Yasuaki Hiraoka, and Kenji Fukumizu. Persistence weighted gaussian kernel for topological data analysis. In *International Conference on Machine Learning*, pages 2004–2013, 2016.
- [33] Austin Lawson. PersistenceCurves (a python package for computing persistence curves). <https://github.com/azlawson/PersistenceCurves>, 2019.
- [34] Svetlana Lazebnik, Cordelia Schmid, and Jean Ponce. A sparse texture representation using local affine regions. *IEEE Transactions on Pattern Analysis and Machine Intelligence*, 27(8):1265–1278, 2005.
- [35] Chunyuan Li, Maks Ovsjanikov, and Frederic Chazal. Persistence-based structural recognition. In *Proceedings of the IEEE Conference on Computer Vision and Pattern Recognition*, pages 1995–2002, 2014.
- [36] Li Li, Wei-Yi Cheng, Benjamin S Glicksberg, Omri Gottesman, Ronald Tamler, Rong Chen, Erwin P Bottinger, and Joel T Dudley. Identification of type 2 diabetes subgroups through topological analysis of patient similarity. *Science translational medicine*, 7(311):311ra174–311ra174, 2015.
- [37] Ce Liu, Lavanya Sharan, Edward H Adelson, and Ruth Rosenholtz. Exploring features in a bayesian framework for material recognition. In *2010 IEEE Computer Society Conference on Computer Vision and Pattern Recognition*, pages 239–246. IEEE, 2010.

- [38] Li Liu, Jie Chen, Paul Fieguth, Guoying Zhao, Rama Chellappa, and Matti Pietikäinen. From bow to cnn: Two decades of texture representation for texture classification. *International Journal of Computer Vision*, 127(1):74–109, 2019.
- [39] Seth Lloyd, Silvano Garnerone, and Paolo Zanardi. Quantum algorithms for topological and geometric analysis of data. *Nature communications*, 7:10138, 2016.
- [40] Yuriy Mileyko, Sayan Mukherjee, and John Harer. Probability measures on the space of persistence diagrams. *Inverse Problems*, 27(12):124007, 2011.
- [41] Takenobu Nakamura, Yasuaki Hiraoka, Akihiko Hirata, Emerson G Escolar, and Yasumasa Nishiura. Persistent homology and many-body atomic structure for medium-range order in the glass. *Nanotechnology*, 26(30):304001, 2015.
- [42] Vidit Nanda. Perseus, the persistent homology software. <http://www.sas.upenn.edu/~vnanda/perseus>, 2013.
- [43] Ippei Obayashi, Yasuaki Hiraoka, and Masao Kimura. Persistence diagrams with linear machine learning models. *Journal of Applied and Computational Topology*, 1(3):421–449, Jun 2018.
- [44] Timo Ojala, Topi Maenpaa, Matti Pietikainen, Jaakko Viertola, Juha Kyllonen, and Sami Huovinen. Outex-new framework for empirical evaluation of texture analysis algorithms. In *Object recognition supported by user interaction for service robots*, volume 1, pages 701–706. IEEE, 2002.
- [45] Steve Oudot and Elchanan Solomon. Inverse problems in topological persistence. *arXiv preprint arXiv:1810.10813*, 2018.
- [46] Michelangelo Paci, Loris Nanni, and Stefano Severi. An ensemble of classifiers based on different texture descriptors for texture classification. *Journal of King Saud University - Science*, 12 2012.
- [47] Jose A Perea and Gunnar Carlsson. A klein-bottle-based dictionary for texture representation. *International Journal of Computer Vision*, 107(1):75–97, 2014.
- [48] Valerie Randle and Olaf Engler. *Introduction to texture analysis: macrotexture, microtexture and orientation mapping*. CRC press, 2014.
- [49] Jan Reininghaus, Stefan Huber, Ulrich Bauer, and Roland Kwitt. A stable multi-scale kernel for topological machine learning. In *Proceedings of the IEEE conference on computer vision and pattern recognition*, pages 4741–4748, 2015.
- [50] Eitan Richardson and Michael Werman. Efficient classification using the Euler characteristic. *Pattern Recognition Letters*, 49:99–106, 2014.

- [51] Bastian Rieck, Filip Sadlo, and Heike Leitte. Topological machine learning with persistence indicator functions. *arXiv preprint arXiv:1907.13496*, 2019.
- [52] Vanessa Robins, James D Meiss, and Elizabeth Bradley. *Computational topology at multiple resolutions: foundations and applications to fractals and dynamics*. PhD thesis, University of Colorado, 2000.
- [53] Mohammad Saadatfar, Hiroshi Takeuchi, Vanessa Robins, Nicolas Francois, and Yasuaki Hiraoka. Pore configuration landscape of granular crystallization. *Nature communications*, 8:15082, 2017.
- [54] L. Sharan, R. Rosenholtz, and E. H. Adelson. Material perception: What can you see in a brief glance? *Journal of Vision*, 14, no. 9, article 12, 2014.
- [55] Katharine Turner, Sayan Mukherjee, and Doug M Boyer. Persistent homology transform for modeling shapes and surfaces. *Information and Inference: A Journal of the IMA*, 3(4):310–344, 2014.
- [56] Afra Zomorodian and Gunnar Carlsson. Computing persistent homology. *Discrete & Computational Geometry*, 33(2):249–274, 2005.

A Elementary Proof of Stability of Persistence Landscapes in Section 3.5

Proof. We need similar estimates to that in Lemma 1. Consider $f(t) = \max_t |\psi_1(t)\chi_{[b_1, d_1)}(t) - \psi_2(t)\chi_{[b_2, d_2)}(t)|$, where $\psi_i(t) = \min\{t - b_i, d_i - t\}$ for $i = 1, 2$. Case 1: $b_1 \leq d_1 \leq b_2 \leq d_2$ and $[b_1, d_1) \cap [b_2, d_2) = \emptyset$. Then

$$f(t) = \begin{cases} \max_{t \in [b_1, d_1)} |\psi_1(t)| = (d_1 - b_1)/2 \leq (b_2 - b_1)/2 \\ \max_{t \in [b_2, d_2)} |\psi_2(t)| = (d_2 - b_2)/2 \leq (d_2 - d_1)/2 \end{cases}. \quad (19)$$

Thus, $f(t) \leq |b_2 - b_1| \vee |d_2 - d_1|$.

Case 2: $b_1 \leq b_2 \leq d_1 \leq d_2$ and $[b_1, d_1) \cap [b_2, d_2) = [b_2, d_1)$. Then

$$f(t) = \begin{cases} \max_{t \in [b_1, b_2]} |\psi_1(t)| \\ \max_{t \in [b_2, d_1)} |\psi_1(t) - \psi_2(t)| \\ \max_{t \in (d_1, d_2)} |\psi_2(t)| \end{cases}. \quad (20)$$

When $t \in [b_1, b_2]$, there are two subcases: $b_1 \leq m_1 \leq b_2$ and $b_1 \leq b_2 \leq m_1$.

$$\max_{t \in [b_1, b_2]} |\psi_1(t)| = \begin{cases} \max_{t \in [b_1, m_1]} t - b_1 = m_1 - b_1 = \frac{(d_1 - b_1)}{2} \\ \max_{t \in [m_1, b_2]} d_1 - t = d_1 - m_1 = \frac{(d_1 - b_1)}{2} \\ \max_{t \in [b_1, b_2]} t - b_1 = b_2 - b_1 \end{cases} \quad (21)$$

Observe that for $b_1 \leq m_1 \leq b_2$, we have $\frac{(d_1 - b_1)}{2} - (b_2 - b_1) = m_1 - b_2 \leq 0$. In each of the cases above, $\max_{t \in [b_1, b_2]} |\psi_1(t)| \leq b_2 - b_1$. Thus, $\max_{t \in [b_1, b_2]} |\psi_1(t)| \leq |b_2 - b_1|$. Similarly, one may verify that when $t \in (d_1, d_2)$, $\max_{t \in (d_1, d_2)} |\psi_1(t)| \leq |d_2 - d_1|$.

When $t \in [b_2, d_1) = [b_1, d_1) \cap [b_2, d_2)$, there are 5 sub cases to consider.

- i) $m_1 \leq b_2 \leq d_1 \leq m_2$;
- ii) $b_2 \leq m_1 \leq d_1 \leq m_2$;
- iii) $m_1 \leq b_2 \leq m_2 \leq d_1$;
- iv) $b_2 \leq m_1 \leq m_2 \leq d_1$;
- v) $b_2 \leq m_2 \leq m_1 \leq d_1$.

One may verify that each case is bounded by $|d_2 - d_1| \vee |b_2 - b_1|$. Therefore, we have

$$\max_{t \in [b_1, d_1) \cup [b_2, d_2)} |\psi_1(t)\chi_{[b_1, d_1)}(t) - \psi_2(t)\chi_{[b_2, d_2)}(t)| \leq |d_2 - d_1| \vee |b_2 - b_1|. \quad (22)$$

□

B More Experimental Results

B.1 Performances of more PCs

Table 5 contains an extensive list of performances with different combinations of curves and machine learning algorithms. Generally speaking, we observe that RF performs better than SVM. The performance of β curves are better than ECC. For the entropy curves **le**, **mle**, **mule**, their performances on both SVM and RF are similar. On the other hand, for the normalized curves **sl**, **sml**, **smul**, the performances of RF are better than those of SVM. In this table, M represents the concatenation of the lifespan, midlife, and multiplicative lifespan curves. Similar to the main text we see that the regular curves are largely unstable across the datasets, dropping in score after we leave Outex. Again, as we saw in the main text, the $S + PS + RF$ curve most often outperforms the other persistence curves proving to be a powerful descriptor. We also note that the entropy curves perform well in general.

B.2 Efficiency

For experimentation purposes, we consider the **mule**. We generate random diagrams in the following way. Each birth value is sampled from a uniform distribution on the interval 0 to 100. To each birth value b , we assign a death value by sampling a uniform distribution on the interval b to 101. We perform two experiments. First, we fix 1000 equidistant points in the interval 0 to 100, and hence $M = 1000$. Second, we vary $\#D$ from the the following set $\{10^3, 10^4, 10^5, 10^6\}$. Finally, to account for statistical errors, we repeat this process 100 times to obtain an average computational time. Table 6 shows results of this experiment. We see computational time has a linear growth in $\#D$.

In the second experiment, we fix $\#D = 1000$ and vary M from the set $\{100, 500, 1000, 5000, 10000, 50000\}$. Again, we repeat this process 100 times to obtain an average computational time. The result is shown in Figure 7. As expected, the computational time has a linear growth in M . These experiments confirm the observation the complexity of computing PC is roughly linear in both threshold and number of generators.

Our Methods	OT0	OT10	UIUC	KTH	FMD
<i>ECC</i> + SVM	92.0	96.4	73.8	78.6	31.0
<i>ECC</i> + RF	96.1	95.0	84.4	89.3	35.8
β + SVM	98.0	97.2	84.5	82.3	31.8
β + RF	97.3	96.0	87.1	90.5	37.2
\mathbf{l} + SVM	96.6	96.1	85.3	83.2	33.2
\mathbf{l} + RF	95.8	94.5	87.3	90.5	35.8
\mathbf{ml} + SVM	97.8	97.0	85.7	82.8	32.1
\mathbf{ml} + RF	97.2	96.5	87.4	90.4	37.4
\mathbf{mul} + SVM	96.2	96.0	87.1	86.4	34.4
\mathbf{mul} + RF	97.1	96.7	86.5	90.6	37.4
\mathbf{M} + SVM	98.1	97.1	87.5	87.8	34.0
\mathbf{M} + RF	97.6	97.2	87.8	91.0	38.4
$\mathbf{M} + PS$ + SVM	98.1	97.1	88.1	87.0	34.5
$\mathbf{M} + PS$ + RF	98.3	97.8	90.3	93.4	40.9
\mathbf{sl} + SVM	95.7	95.7	88.4	89.2	39.5
\mathbf{sl} + RF	96.8	94.7	92.9	93.8	40.2
\mathbf{sml} + SVM	93.2	95.0	83.6	80.8	39.8
\mathbf{sml} + RF	97.3	96.5	91.2	91.3	39.2
\mathbf{smul} + SVM	92.9	94.1	87.7	86.6	41.4
\mathbf{smul} + RF	96.8	96.2	92.3	91.7	40.6
\mathbf{S} + SVM	96.7	96.3	92.4	94.3	41.5
\mathbf{S} + RF	98.3	97.2	93.5	93.1	41.8
$\mathbf{S} + PS$ + SVM	95.1	94.8	88.9	94.8	31.9
$\mathbf{S} + PS$ + RF	98.5	97.7	93.5	94.4	43.6
\mathbf{le} + SVM	96.6	96.6	91.1	91.2	34.5
\mathbf{le} + RF	96.9	94.2	92.2	92.7	40.9
\mathbf{mle} + SVM	97.2	96.4	90.5	86.1	35.0
\mathbf{mle} + RF	97.4	96.5	91.1	91.0	35.5
\mathbf{mule} + SVM	97.3	96.6	91.9	90.1	38.5
\mathbf{mule} + RF	97.4	96.6	91.8	91.4	35.7
\mathbf{E} + SVM	97.7	97.3	92.9	94.3	39.5
\mathbf{E} + RF	98.3	97.3	92.7	93.0	41.6
$\mathbf{E} + PS$ + SVM	95.9	96.1	92.8	95.8	33.7
$\mathbf{E} + PS$ + RF	98.5	97.6	93.2	93.7	42.3
$\mathbf{E} + S$ + SVM	97.7	97.3	92.8	94.3	39.6
$\mathbf{E} + S$ + RF	98.3	97.2	92.9	93.2	42.0
$\mathbf{E} + S + PS$ + SVM	95.9	96.1	92.2	95.9	33.7
$\mathbf{E} + S + PS$ + RF	98.5	97.4	93.2	93.2	42.3

Table 5: Performance on Outex, UIUCTex, KTH-TIPS, and FMD. Hightlighted are the best performance in this table.

Diagram points	10^3	10^4	10^5	10^6
Time (seconds)	0.007	0.068	0.719	6.735

Table 6: Computational time for **mule** with the fixed number of mesh points $M = 10^3$.

Mesh points	100	500	1000	5000	10000	50000
Time (seconds)	0.026	0.045	0.068	0.240	0.452	2.141

Table 7: Computational time for **mule** with the fixed number of points in the persistence diagram $\#D = 100$.

C Texture Images



Figure 5: The 25 textures in UIUCTex.

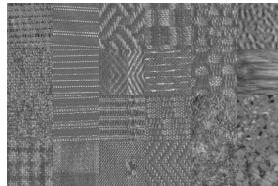


Figure 6: The 24 textures in Outex.

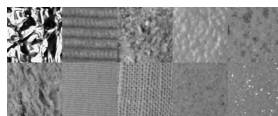


Figure 7: The 10 textures of KTH-TIPS.



Figure 8: The 10 textures in the FMD database.